This document is the accepted manuscript version of the following article:

Senocrate, A., Bernasconi, F., Rentsch, D., Kraft, K., Trottmann, M., Wichser, A., … Battaglia, C. (2022). Importance of substrate pore size and wetting behavior in gas diffusion electrodes for CO2 reduction. ACS Applied Energy Materials. https://doi.org/10.1021/acsaem.2c03054

The importance of substrate pore size and wetting behavior in gas diffusion electrodes for CO_2 reduction

Alessandro Senocrate, Francesco Bernasconi, Daniel Rentsch, Kevin Kraft, Matthias Trottmann, Adrian Wichser, Davide Bleiner, and Corsin Battaglia*

Empa, Swiss Federal Laboratories for Materials Science and Technology, Überlandstrasse 129, 8600 Dübendorf (CH)

*alessandro.senocrate@empa.ch

Keywords: substrate, CO_2 reduction, electrocatalysis, gas diffusion electrodes, hydrophobicity, pore size, wetting

Abstract

We study the effect of substrate pore size and wetting behavior on the performance of polymer-based Ag gas diffusion electrodes (GDEs) for electrochemical CO_2 reduction. We find a strong correlation between the pore size of the substrate and the GDE product selectivity and performance stability during CO_2 electrolysis. We attribute this correlation to the GDE's wetting behavior, in particular to its resistance to aqueous electrolyte penetration. We quantify this resistance by the water entry pressure, i.e. the minimum pressure required to push water through a hydrophobic porous substrate, which depends on the pore size of the substrate and on the hydrophobicity of the substrate polymer. While substrates with low water entry pressure yield GDEs that exhibit poor CO selectivity and stability, high water entry pressure substrates lead to greatly improved Faradaic efficiency towards CO (up to 95 % at 100 mA/cm^2) and remarkably longer performance stability (97 % of initial CO selectivity retained after >40 hours). We also assess the sensitivity to surface Cu contaminants and find that substrates with high water entry pressures lead to GDEs that are more resilient to impurities, with an almost unvaried selectivity even when contaminated with > 1 at % Cu vs Ag. On this basis, we propose the water entry pressure as a metric to assess GDE quality. These results highlight how acting on the substrate is a powerful and scalable handle for improving the performance of GDEs for the electrochemical CO_2 reduction.

Introduction

Electrochemical CO_2 reduction (CO_2RR) to produce synthetic fuels and chemical precursors is emerging as a highly promising pathway to abate carbon emissions and move closer to a circular carbon economy. Given the severity of climate change, and the progressively more stringent targets for energy efficiency and CO_2 emissions,[1,2] significant efforts are directed towards understanding the catalytic processes underlying CO_2RR, and towards practically implementing this technology.

An important aspect is to develop catalysts that are highly active, yield the desired product(s) with high selectivity, and retain these properties for an extended period. Activity refers to the ability of a catalyst to achieve high current densities at a given applied voltage, while selectivity relates to the fraction of specific product(s) in the total products mix. In general, CO_2RR electrocatalysts show a complex product distribution, in the simplest case yielding simultaneously CO via the CO_2RR, and H_2 from the com-

peting parasitic hydrogen evolution reaction (HER), the latter tending to increase over time.[3–6] In order to steer CO_2 electrolysis towards a desired product distribution, common approaches include changing the catalyst,[7,8] the cations and anions in the electrolyte,[9–12] the electrolyte pH,[13,14] or even the architecture of the electrolysis cell.[15] To reach current densities ≥ 200 mA/cm^2 identified by techno-economic analyses as a requirement to compete with traditional fuel production routes,[16–18] gas diffusion electrodes (GDEs) are currently investigated intensively.[19–26]

GDEs reduce mass transport limitations associated with the low solubility of CO_2 in aqueous electrolytes by providing gaseous CO_2 to -and near- the catalyst. Most studies to date use carbon-based GDE substrates, despite their participation in GDE flooding by the electrolyte and subsequent degradation of activity and selectivity.[27,28] To prevent flooding and achieve stable CO_2RR, a new class of GDEs based on hydrophobic polymer substrates coated with a sputtered metal catalyst has been recently developed.[20,21,24,25] These have attracted great attention due to their outstanding CO_2RR activity and selectivity. So far, a number of different explanations have been proposed to explain their excellent performance, including the formation of abrupt gas-liquid interfaces,[25] an optimized combination of catalyst and ionomer mixture,[21] and advanced electrolyzer design.[24]

In contrast to previous studies, we focus our attention on the properties of the GDE polymer substrate itself. We demonstrate that product selectivity, performance stability, and resilience to impurities of Ag GDEs are all strongly affected by the pore size of the GDE substrate, providing a scalable strategy to improve performance. We correlate these key performance indicators to the substrate's wetting behavior, in particular to its resistance to aqueous electrolyte penetration, which is a function of the substrate pore size and of the hydrophobicity of the substrate polymer. This resistance is quantified by the water entry pressure (WEP), i.e. the minimum pressure necessary to force water through a hydrophobic porous substrate, which we advocate as an important metric to assess GDE quality.

We show that GDEs with low WEP, e.g. ~0.5 bar, show inferior selectivity towards CO (< 30 % at 100 mA/cm^2) as well as low stability (only 65 % of initial selectivity towards CO retained after 3 hours electrolysis). In stark contrast, GDEs with higher WEPs, e.g. > 5 bar, yield remarkably high selectivity towards CO (up to 95 % at 100 mA/cm^2) and long-term stability (~97 % of initial selectivity towards CO retained after > 40 hours electrolysis). This corresponds to a multi-fold improvement of the GDE selectivity and stability obtained solely by acting on the substrate and ensuring a high WEP. Remarkably, these FE_{CO} values are amongst the best reported for Ag GDEs using neutral electrolytes, and can even compete with values obtained using alkaline electrolytes.[6,9,20,29–31] We therefore rationalize the exceptional performance previously reported for these types of GDEs[20,21,24,25] in the context of the substrates used, which in all cases consisted of highly hydrophobic substrates with small pore sizes, resulting in high WEP.

Results

We consider two sets of commercial polymer fiber substrates, composed of polytetrafluoroethylene (PTFE) or polyvinylidenefluoride (PVDF) with different pore sizes in the range of 0.2 µm to 3 µm (details are given in Table S1, Supporting Information). The substrates are used as obtained to fabricate GDEs by sputtering on one side a conductive Ag layer with a nominal thickness of 500 nm, as measured on a flat non-porous reference substrate (nominal loading ~ 0.5 mg Ag / cm^2). **Fig. 1** reports microstructural and structural characterization of the uncoated polymer substrate and of the GDEs employing porosimetry and scanning electron microscopy (SEM) images. From porosimetry, the mean pore sizes are 0.3, 0.4, and 2.8 µm for PTFE substrates (Fig. 1a), and 0.3, 0.4, and 0.8 µm for PVDF substrates (Fig. 1b). As shown in Fig. S3 in the Supporting Information, no significant changes in the pore size distribution are observed after the deposition of the metal catalyst. After sputtering deposition of the Ag catalyst, all GDEs show X-ray reflections belonging only to the Ag metal and, in the case of PTFE substrates, to the substrate itself (Fig. S4).

A comparison between top down SEM images of a PTFE and PVDF substrates with similar pore size (given in Fig. 1c and 1d, and more completely in Fig. S5) reveals a different 'weaving' structure of the fiber substrates, which is expected due to the different fabrication routes (stretching and fibrillation of PTFE, and electrospinning of PVDF). Analysis of the cross sections given in Fig. 1e and 1f, obtained by focused ion beam, shows that that in these GDEs, the relatively directional nature of the sputtering deposition used introduces the catalyst only on one side of the substrate, and yield a porous but interconnected metal layer that mimics the underlying fibrous structure. Below this metal layer, the polymer fibers appear –if at all- only partially coated, thus retaining their hydrophobic nature and allowing the substrate properties to exert an effect on the GDE.

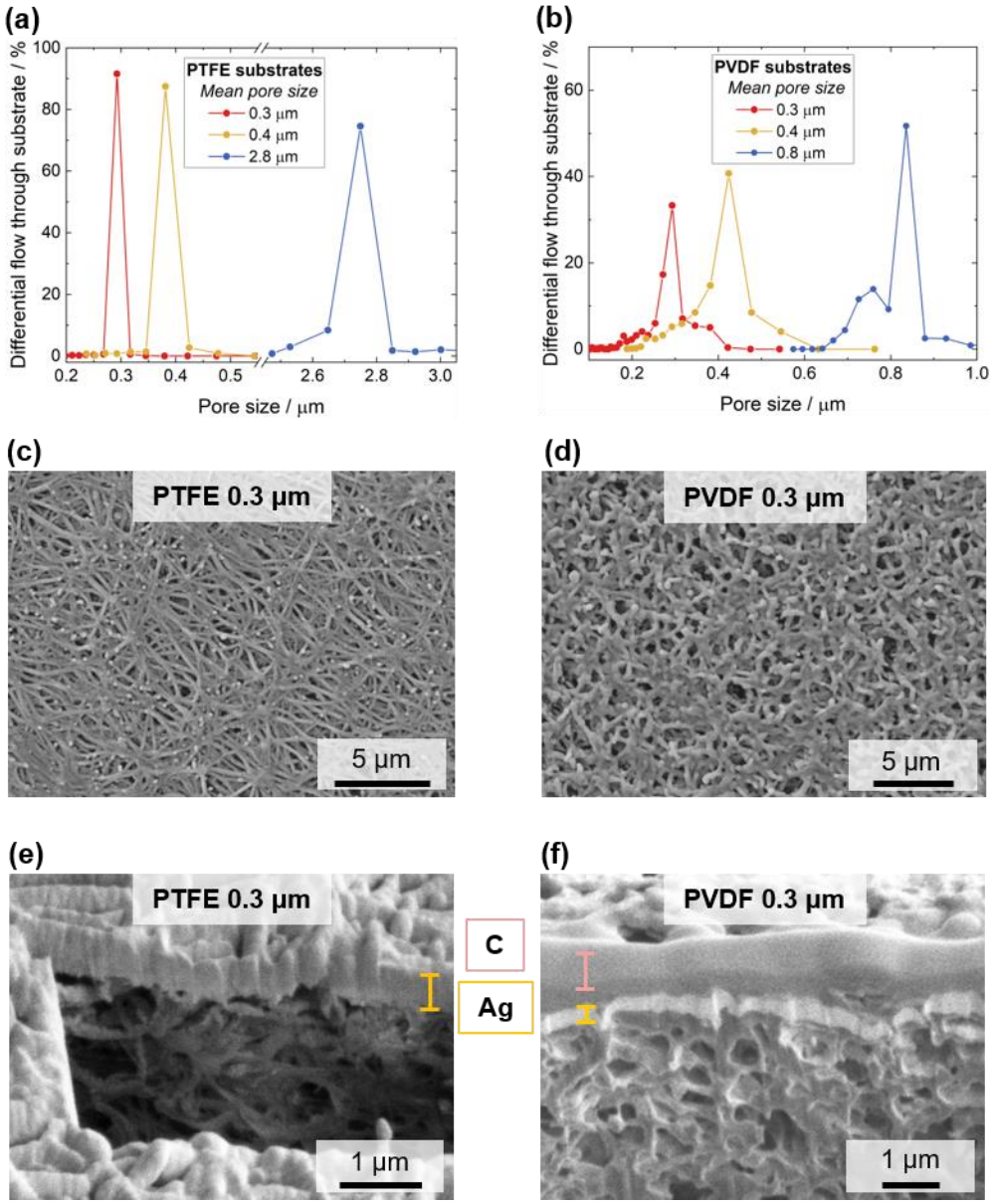

Figure 1. Microstructural characterization of the PTFE and PVDF fiber substrates. **(a), (b)** Porosimetry measurements for PTFE and PVDF substrates of various pore sizes. **(c), (d)** top down SEM image and **(e), (f)** cross sectional SEM image of Ag-deposited GDEs with 0.3 µm mean pore size, fabricated on a PTFE or PVDF substrates. The PVDF-based GDE was protected with a carbon layer (highlighted in pink) before milling the cross section.

We then analyze the catalytic activity and selectivity of the GDEs using a 3-compartment electrolysis cell (schematic design given in Fig. S1, Supporting Information). One compartment is used to supply gaseous CO_2 to the GDE acting as cathode, while the other two compartments (catholyte and anolyte chambers) are separated by a Nafion membrane and filled with a 1M $KHCO_3$ electrolyte, saturated with CO_2. Nafion is chosen for its good stability and high conductivity in neutral pH, and to avoid carbonate crossover to the anodic side leading to CO_2 losses. To complete the electrochemical cell, an IrO_x catalyst electrodeposited on a Ti grid is immersed into the anolyte and used as anode for the oxygen evolution reaction. The anode is oversized more than 10 times as not to limit the cathode's performance.

Fig. 2 reports the Faradaic efficiency (FE) of gaseous products as a function of total current density for Ag-coated PTFE- and PVDF-based GDEs with different pore sizes. For clarity, we plot only the Faradaic efficiency (FE) of the gaseous products determined by gas chromatography. FE values are normalized to facilitate comparison between GDEs, with the normalization accounting for all detected products, gaseous and liquid, the latter determined by nuclear magnetic resonance. The normalization does not affect the observed trends. The complete, non-normalized product distribution, which includes liquid HCOOH, is given in Fig. S6, while Fig. S7 shows the reproducibility of the catalytic performance measurements.

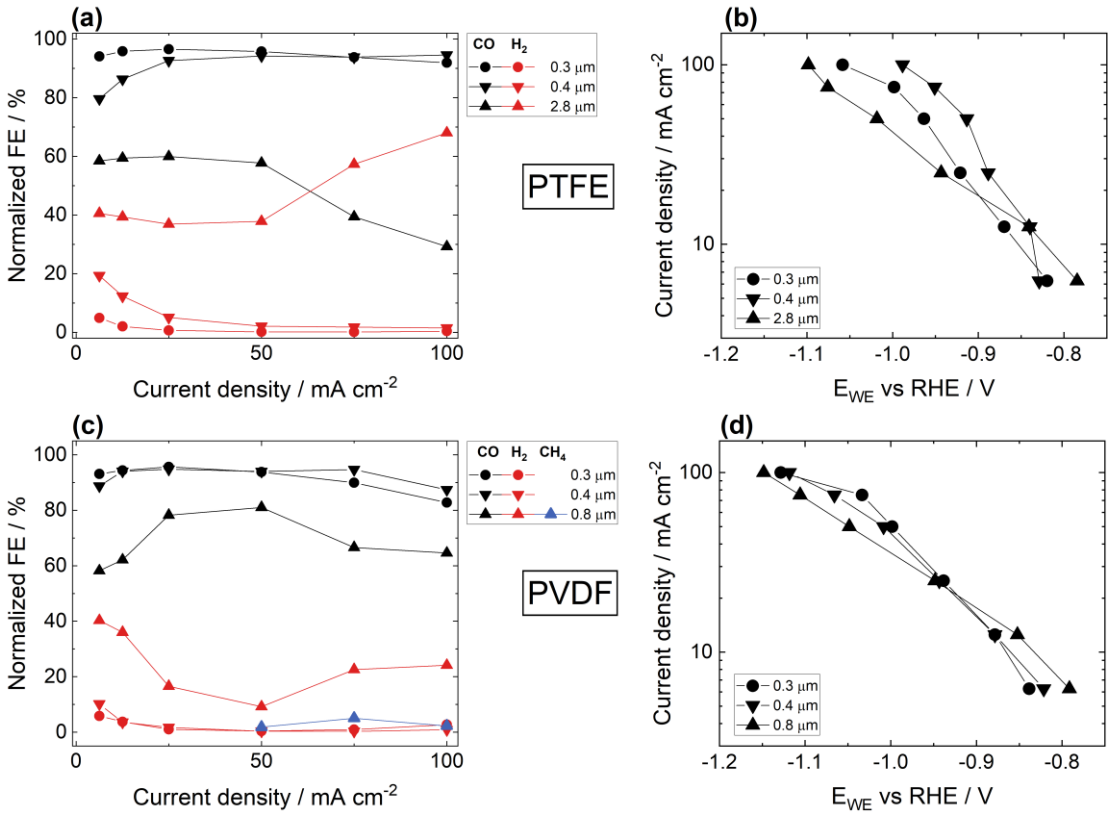

Figure 2. Microstructural effect on the selectivity of Ag catalysts deposited on PTFE and PVDF substrates. Normalized CO and H_2 Faradaic efficiencies as a function of current for Ag catalysts deposited on **(a)** PTFE substrate and **(c)** PVDF substrates of different pore sizes. Current voltage curve for the same catalysts on **(b)** PTFE substrates and **(d)** PVDF substrates. The FE values plotted are the average over a 1 h electrolysis experiment at constant current.

Inspection of Fig. 2a and 2c shows that GDEs with larger pore size generally yield a lower FE towards CO and a higher FE towards H_2, irrespective of the nature of the substrate polymer. For example, at the highest current density of 100 mA/cm^2, GDEs with large mean pore sizes of 2.8 µm for PTFE and 0.8 µm for PVDF reach only FE_{CO} ~30% and ~65 %, respectively, i.e. below what is typically reported for Ag-based catalysts.[20,29,30] However, GDEs with a smaller mean pore sizes of 0.3 and 0.4 µm reach a much higher normalized FE_{CO} > 80 % for both PTFE and PVDF substrates at the same current density. Remarkably, the PTFE-based GDE with 0.4 µm pores achieves a FE_{CO} value of 95 %, which is amongst the highest reported for Ag GDEs using neutral electrolytes, and even competes with values obtained using basic electrolytes.[6,9,20,29–31]

As expected, FE_{H2} shows the opposite behavior to FE_{CO}, with high FE_{H2} values obtained for larger substrate pore sizes. Considering formic acid, FE_{HCOOH} shows only a weak dependence on substrate pore size (Fig. S6 in the Supporting Information). Smaller pore sizes, for both PVDF and PTFE substrates, seem to lead to higher FE_{HCOOH} at high current densities, while at lower current density the values are comparable for different pore sizes. This is consistent with reports indicating strongly alkaline conditions, generated under high currents thanks to proton consumption, as the cause for the shift towards formic acid production.[29,32]

The above results highlight a massive selectivity improvement, e.g. a multi-fold increase in FE_{CO}, obtained solely by acting on the GDE substrate. Given the importance of this result, it is crucial to rule out other potential causes for the observed selectivity variations. As shown in Fig 2b and 2d, GDEs with drastically different selectivity show similar voltage values and current-voltage slopes, indicating that there is no additional overpotential responsible for these selectivity variations. Additionally, electrochemically active surface area (ECSA) measurements carried out before and after the electrolysis experiment, show highly comparable surface areas (Table S2 of the Supporting Information), which in all cases slightly increase after electrolysis, ruling out ECSA as the cause for the difference in performance. Thus, we attribute the strong selectivity changes to the substrate microstructure. The GDE substrates not only have different pore sizes, but also different thicknesses ranging from 25 to 300 µm (Table S1). However, we find that the product selectivity does not depend on GDE thickness in the range 20-450 µm (Fig. S8, Supporting Information), thus we can unambiguously attribute the observed changes to the substrate pore size.

To investigate more in detail the influence of GDE wetting and decouple it from other effects that could be caused by different substrate pore sizes, we also analyze a GDE based on a PTFE substrate with a small pore size of 0.3 µm, which is commercially available in hydrophilic form (obtained through an undisclosed surface treatment). As shown in Fig. 3, the hydrophilic PTFE-based GDE shows a drastically different product selectivity than a hydrophobic GDE of comparable pore size (plotted again here for better comparison), with FE_{CO} rapidly decaying with increasing current density. The decay is even more pronounced than for the PTFE GDE with the largest mean pore sizes of 2.8 µm (compare with Fig. 2a and 2c). This highlights the relevance of the GDE's wetting behavior in determining the product selectivity for CO_2RR.

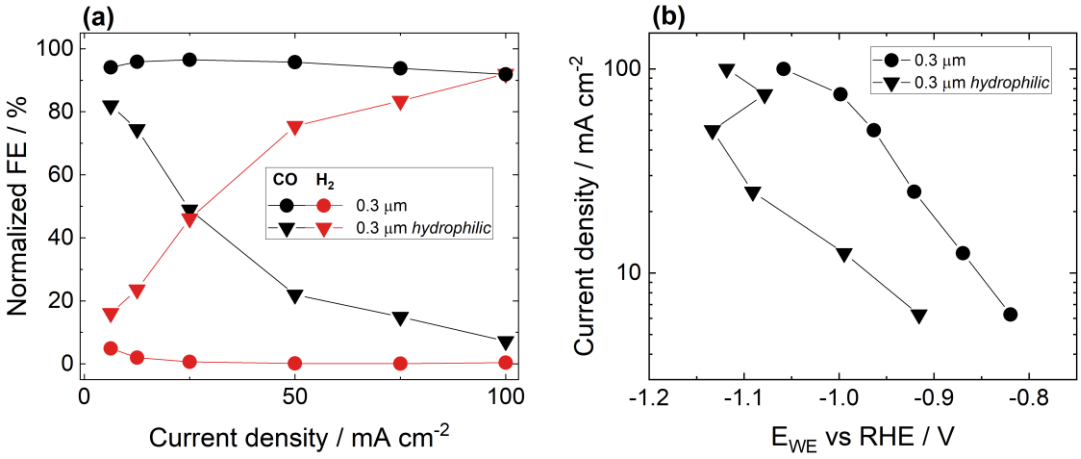

Figure 3. (a) Normalized CO and H_2 Faradaic efficiencies as a function of current density for an GDE made of Ag deposited on a PTFE substrate with 0.3 µm pore size, which has been surface-treated to be hydrophilic. For comparison, a GDE made from Ag deposited on a hydrophobic PTFE substrate with 0.3 µm pore size is given. **(b)** Current voltage curve for the same GDEs. The FE values plotted are the average over a 1 h electrolysis experiment at constant current.

To provide a quantitative measure of the wetting behavior of our fibrous, porous GDEs when in contact with the aqueous electrolyte, we cannot rely on contact angle measurements, as these require flat and compact surfaces. We also cannot measure the electrolyte seepage rate through the GDE, as done for carbon paper substrates,[33,34] because the hydrophobic nature of the polymer substrates prevent any seepage even in the event of catalyst degradation. In this regard, the water entry pressure (WEP), i.e. the pressure necessary to push water through an initially dry, hydrophobic, porous material, provides a better indication of the substrate wetting behavior and captures the fact that substrates made from the same polymer but with different pore sizes are differently able to resist water/ aqueous electrolyte penetration. We therefore carried out WEP measurements for all of our GDE substrates, which are shown in Fig. S9, Supporting Information. As expected, substrate of the same polymer with smaller pore sizes show a much higher WEP than their larger pore counterpart. For similar pore sizes, PTFE substrates have a much larger WEP than PVDF analogues, due to their higher water contact angles (water contact angles for bulk PTFE and PVDF are > 120° [35] and 90° [35,36] respectively). Despite its small 0.3 µm pore size, the surface-treated hydrophilic PTFE substrate shows no resistance to wetting with a WEP of ~0 bar, in contrast to the hydrophobic 0.3 µm PTFE substrate boasting a WEP of 9.2 bar. We also verified that the WEP values are unchanged when using 1 M $KHCO_3$, i.e. our CO_2RR electrolyte, as a measurement fluid (Section 9, Supporting Information).

Having quantified the GDE's wetting behavior with the electrolyte, we relate it to their catalytic performance in the CO_2RR. Fig. 4a shows that the Faradaic efficiency towards CO correlates strongly with the WEP, with higher WEP substrates yielding GDEs with higher FE_{CO}, irrespective of the underlying chemical nature of the substrate polymer. This result is consistent with improvements in CO_2RR selectivity reported when using hydrophobic catalyst binders or applying a hydrophobic polymer layers on top of

the catalyst.[21,25,37,38] Concerning stability, in Fig. 4b we compare how FE_{CO} evolves with time for GDEs with different WEP during electrolysis at 100 mA/cm^2. The stability of the FE_{CO} clearly correlates with WEP, with GDEs boasting the highest WEPs, namely the ones based on PTFE with 0.3 and 0.4 µm pore size, showing no FE_{CO} decay after 3 h electrolysis. Instead, FE_{CO} decays more rapidly for the others, with the fastest decay observed for the GDE based on the hydrophilic polymer substrate with the lowest WEP of ~0 bar, despite its small mean pore size of 0.3 µm. These findings are a clear indication that the loss of CO selectivity is due to flooding of the catalyst with electrolyte, which inhibits CO_2 supply to the catalyst. ECSA measurements carried out at the beginning of the electrolysis, and then every subsequent hour (indicated by dashed lines in Fig. 4b), show a moderate increase in surface area for all GDEs during operation, with negligible differences amongst the GDEs (Table S2, Supporting Information). However, due to the non-conductive nature of our GDE substrates, such ECSA changes are not direct evidence of an increased wetting or a flooding process, but are more likely caused by compositional changes within the electrolyte or possibly mild surface reconstruction. A more detailed discussion of this aspect is given in Section 5, Supporting Information.

Noting the promising stability of GDE with high WEP, we then carry out a long-term electrolysis experiment. Fig. 4c shows that a GDE based on a PTFE substrate with 0.3 µm pore size, boasting the highest WEP of 9.2 bar, retain more than 97 % of its original FE_{CO} after a > 40 h experiment, and does not show shifts in the cathode voltage beside an initial activation. This indicates a stable and well-attached catalyst layer, and underlines the potential of this class of GDEs for practical applications.

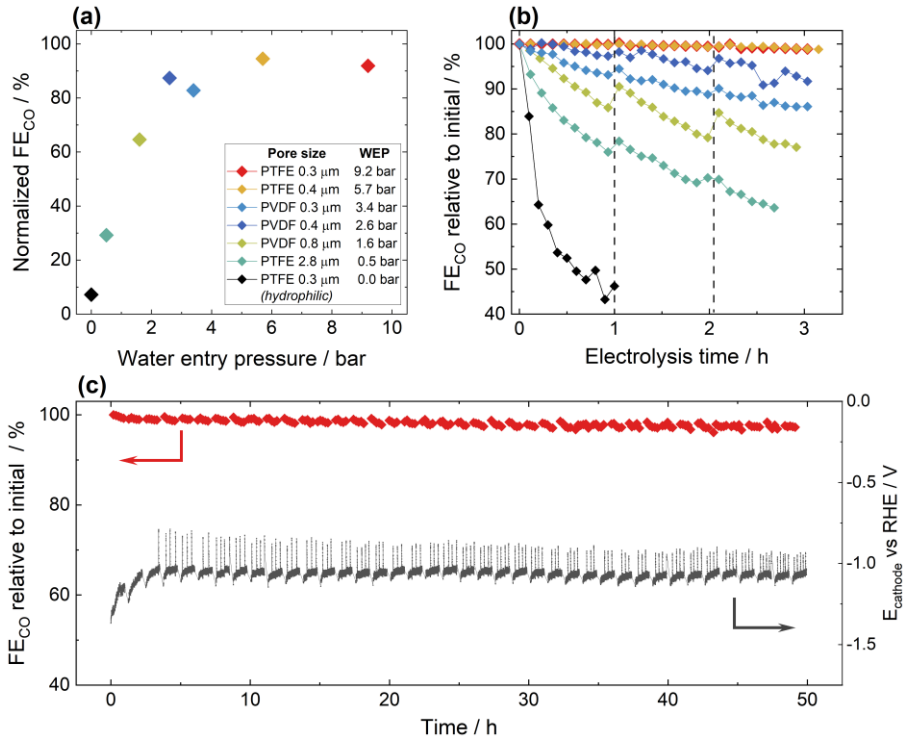

Figure 4. (a) Normalized CO Faradaic efficiency at 100 mA/cm^2 for all GDEs analyzed in this work as a function of their water entry pressure. PVDF and PTFE substrates are marked in different colors. **(b)** Stability of CO Faradaic efficiency relative to the initial value during an electrolysis experiment at 100 mA/cm^2 for GDEs of different water

entry pressures. The GDE based on PVDF with 0.4 µm pore size retains more FE_{CO} than expected from its WEP. The dashed lines indicate interruption of the electrolysis experiment to measure ECSA, which takes place around 0 V_{RHE} for 20 min. Partial recovery of the FE_{CO} can be attributed to changes in the local environment, such as lower local electrolyte temperatures leading to higher CO_2 solubility. **(c)** Long-term stability of an Ag GDE based on PTFE substrate with 0.3 µm pore size (WEP = 9.2 bar). Every hour, the electrolysis is interrupted for ~15 min to avoid local catalyst heating, yielding a total electrolysis time of 41 hours. Complete, non-normalized product distribution data and cathode voltages are given in Fig. S11 and S12 and S13 of the Supporting Information.

An additional notable point concerns resilience to impurity. As seen in Fig. 2c, the Ag GDE based on PVDF substrate with 0.8 µm pore size shows a perceptible selectivity for CH_4 at current densities above 50 mA/cm^2, with FE_{CH4} between 1 % and 5 %. In contrast, GDE based on a PTFE substrate with similar mean pore size of 0.4 µm show no FE_{CH4}. Note that, despite similar pore sizes, the PVDF and PTFE substrates show rather different WEPs, namely 1.6 bar and 5.7 bar respectively. The CH_4 production on the PVDF GDE could indicate the presence of a catalytically active impurity, even though PVDF and PTFE substrates underwent catalyst deposition in the same batch, to minimize variations. We thus analyze the chemical composition of nominally pure Ag GDEs, in particular their metallic contamination content, by X-ray fluorescence (XRF) and laser-ablation inductively-coupled-plasma mass spectroscopy (LA-ICP-MS) analysis, the latter having a detection limit in the ppm range. The analysis and related discussion, including the investigation of potential oxygen and sulfur contaminations is given and discussed in Supporting Information, Section 10.

The PTFE- and PVDF-based GDEs do not show significant differences in their composition, in principle ruling out impurities as a cause for their different selectivity. In addition, we note that CH_4 selectivity on pure Ag catalysts under high overpotential has been reported before, and this could also be the case here.[39] Nonetheless, we investigated the consequences of a potential Cu contamination, as Cu is present in our sputtering system and it is a catalyst known to have a strong CH_4 selectivity. We systematically investigate the FE_{CH4} of a set of PVDF and PTFE substrates of 0.8 and 0.4 µm pore size respectively, coated with a base layer of Ag with a nominal thickness of 500 nm and subsequently decorated with different amounts of sputtered Cu, with a nominal thickness ranging approximately from 0.2 nm (0.04 at. % vs Ag) to 10 nm (1.1 at. % vs Ag). To ensure exactly the same amount of Cu, we coat PVDF and PTFE substrates side by side, and assess their Cu content with LA-ICP-MS (Table S3 and Fig. 5). Fig. 5 shows that, during CO_2 reduction, the two different substrates lead to a drastically different behavior, with high WEP PTFE-based GDEs behaving largely like pure Ag (FE_{CO} > 80%, Fig. 5a) and lower WEP PVDF-based GDEs showing a substantial FE_{CH4} which strongly increase with Cu content. Notably, FE_{CH4} exceeds 35 % at a Cu content of 1 % at. vs Ag (Fig. 5b).

The strong difference in FE_{CH4} for the Cu-contaminated PVDF- and PTFE-based GDEs could also explain the different selectivity observed in nominally pure Ag GDEs, which according to LA-ICP-MS both contain a minor amount of 0.002 % at. Cu vs Ag (Table S4 in the Supporting Information). Nonetheless, we cannot rule out that the CH_4 selectivity of nominally pure GDEs stems from other impurities instead of

Cu. In any case, the picture that emerges is that the impurity resilience of the GDEs is also dependent on substrate pore size and wetting behavior, an aspect that should be taken into account whenever analyzing different microstructures, especially when impurities are expected or when preparing complex (e.g. bimetallic) catalysts.

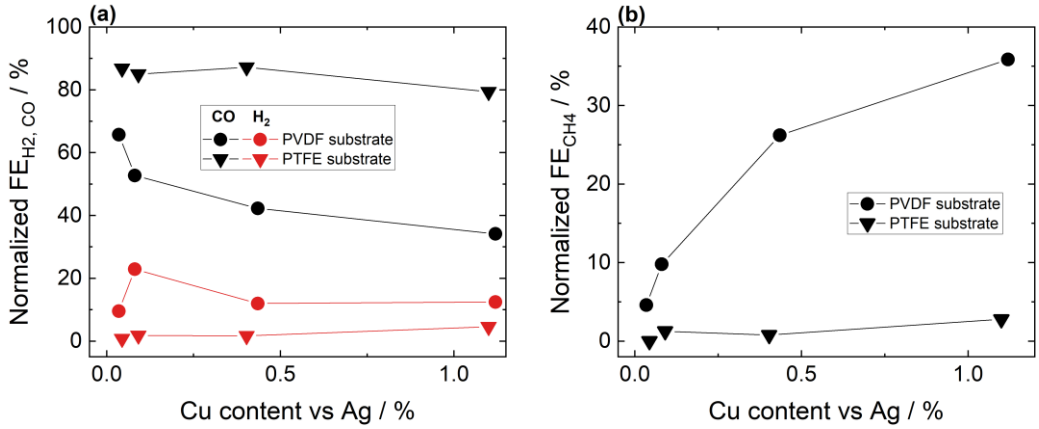

Figure 5. Normalized FE of GDEs composed of PTFE or PVDF substrates with 0.4 and 0.8 µm pore size respectively, sputtered with Ag and subsequently with a controlled amount of Cu impurities. **(a)**. FE for CO and H_2 as a function of Cu atomic content vs Ag, obtained as an average over a 1 h electrolysis experiment at 100 mA/cm^2 in 1 M $KHCO_3$. **(b)**. FE for CH_4 as a function of Cu content, obtained as an average over a 1 h electrolysis experiment at 100 mA/cm^2 in 1 M $KHCO_3$. Complete, non-normalized product distribution with additional products showing FE >1 % is given in Fig. S14.

Discussion

The Ag GDEs studied here mostly yield only H_2 and CO from the HER and CO_2RR, with larger pore size substrates favoring H_2 production, and smaller pore size substrates favoring CO (Fig. 2). A potential explanation for our findings is that different pore sizes affect the local reagent and product concentrations near the catalyst, favoring HER over CO_2RR or vice versa.[40–46] Previous reports have also studied the effect of pore sizes in nanostructured Cu catalysts,[42] or the effect of cavity size on laser-ablated Cu foils,[40] in both cases using electrodes immersed in the electrolyte. However, the use of GDEs and the wide substrate pore sizes considered here (300-3000 nm) are unlikely to hinder the access of gaseous CO_2, nor the removal of gaseous products from the GDE. This is even more the case for the substrates with larger pores, which nonetheless show a lower FE_{CO}, ruling out gaseous CO_2 access as the reason for the difference in selectivity.

Still, the polymer substrates influence the wetting behavior of the GDEs with the electrolyte, which is not only responsible for providing H_2O to the catalyst active sites, but also strongly affects CO_2 supply. The comparison between the surface-treated hydrophilic GDE and its hydrophobic counterpart (Fig. 3) shows a much larger FE_{H2} and a lower FE_{CO} upon facilitating the GDE wetting, confirming the direct role of the electrolyte in affecting selectivity. Indeed, gaseous CO_2 can readily reach the catalyst only in the areas not covered by the electrolyte, i.e. in the triple-phase boundaries between electrolyte, catalyst, and gas phase, which are small in number and thus not expected to contribute significantly to the

overall product generation.[47] Conversely, to reach the catalyst in the areas covered by the electrolyte, CO_2 must dissolve and diffuse in the liquid phase, reacting at the double phase boundaries between electrolyte and catalyst, which are much more abundant and thus generate a higher quantity of products.[47]

In this latter case, the electrolyte coverage, and more specifically, the thickness of the electrolyte layer covering the catalyst is the key parameter that affects the diffusion path of dissolved CO_2 from the gas phase to the catalyst. Unfortunately, the lack of suitable experimental techniques makes it extremely challenging to obtain any experimental evidences on electrolyte layer thickness. Nonetheless, we expect this thickness to depend on the wetting behavior of the GDEs, as measured by the WEP. The rationale is that our GDEs, as visible in the cross sections of Fig. 1e and 1f, are composed of a porous Ag layer resting on top of an uncoated or partially uncoated polymer substrate, and as such mix hydrophilic Ag-coated sections with uncoated hydrophobic areas. The electrolyte can easily wet and seep through the porous Ag layer, but the extent of its penetration within the underlying polymer layer will depend on substrate WEP. Decreasing WEP will lead to a more pronounced electrolyte penetration within the polymer layer, to a thicker electrolyte layer facing the gas phase, and thus to a longer diffusion path for dissolved CO_2 before it can reach the catalyst. Combined with high CO_2 consumption due to the CO_2RR, this leads to a promotion of the HER due to scarce CO_2 availability. This is in agreement with previous studies on the beneficial effect of hydrophobicity on CO_2 electrolysis, obtained e.g. by using hydrophobic catalyst binders.[21,25,34,37,38,48] We recognize that, for larger pore sizes, metal deposition through the pores and into the substrate could take place to a perceptible extent, yielding an enhanced wetting behavior in those areas that would further facilitate electrolyte penetration. Nonetheless, such metal patches located deeper into the substrate are unlikely to have a continuous electrical connection to the top catalyst layer, which is the electrical point of contact for the GDE, and as such will not directly contribute to the electrocatalytic reaction. In addition, electrowetting and capillary phenomena, common to carbon-based substrates, are not expected to play a significant role in our GDEs due to the clear interface between the conductive, hydrophilic catalyst layer where those phenomena can take place, and the insulating, hydrophobic substrate.

We therefore explain the lower FE_{CO} of GDEs with large pore, low WEP substrates (Fig. 2a, 2c) in the context of a more pronounced electrolyte penetration within the GDE and of a thicker electrolyte layer. These aspects also explain the different FE_{CO} trends observed as a function of current density (Fig. 2a, 2c). For large pore size, low WEP substrates, rapid GDE flooding and a thicker electrolyte layer strongly prevent access of CO_2 to the catalyst's active sites. This mechanism becomes more evident at higher current density in the form of a decrease in FE_{CO}, due to accelerated depletion of dissolved CO_2 (Fig. 2a, 2c, pore size of 0.8 and 2.8 µm). In contrast, a thinner electrolyte layer, such as the one that can be obtained in small pore size GDEs with high WEP, offers sufficient supply of CO_2 also at higher current

density, due to the proximity of the CO_2 reservoir, i.e. the gas phase. This yields a flatter dependence of FE_{CO} with current density (Fig. 2a, 2c, pore size of 0.3 and 0.4 µm). Additionally, in a thinner electrolyte layer, the local pH buffering capability of the electrolyte during electrolysis will be more limited, due to the lower quantity of electrolyte available close to the catalyst active sites. This will cause more severe shifts to higher pH (i.e. higher local alkalinity) in the proximity to the catalyst's active sites, which in turn favors the CO_2RR by suppressing the HER. The opposite situation, namely lower local alkalinity under reducing conditions apply to a thicker water layer. This is again consistent with the FE_{CO} trends vs current density of Fig. 2a and 2c.

Considering the observed impurity resilience, FE_{CH4} as high as 35 % is obtained in a GDE contaminated with 1.1 % at. Cu, fabricated on a PVDF substrate with an intermediate WEP of 1.5 bar (Fig. 5b). GDEs with higher WEP, in contrast, show a selectivity similar to pure Ag at the same contamination level (Fig. 5b). This finding can also be explained in the context of the electrolyte layer thickness. Lower WEP and a thicker electrolyte layer means less alkaline pH shift, as well as longer dissolved CO_2 diffusion path and thus scarcer local CO_2 availability at high current density. These are the conditions for improved CH_4 production on Cu.[41,49] Oppositely, GDEs with higher WEP and thus a thinner electrolyte layer show a stronger alkaline shift and thus lower proton availability, which can suppress FE_{CH4}.

Conclusions

In conclusion, we showed for the first time that acting on the GDE substrate is a practical and scalable strategy to control and improve selectivity, performance stability, and impurity resilience of GDEs for CO_2RR. In particular, the substrate pore size plays a pivotal role in influencing the GDE's wetting behavior, in particular its ability to resist aqueous electrolyte penetration, which we quantify via the WEP measurement. In general, a higher WEP (i.e., a more hydrophobic substrate and a smaller pore size) leads to substantial improvements in CO_2RR performance, up to a remarkably high FE_{CO} (95 % at 100 mA/cm^2) and long stability (97 % of initial CO selectivity retained after >40 hours). Due to its importance, we advise to add the WEP as a routine characterization whenever fabricating GDEs for CO_2RR. This measurement will not only provide important information on the quality of the GDE, but could also be used to observe changes with pre-treatments or electrolysis time. It will therefore help identifying prominent failure mechanisms and accelerate future developments of CO_2 electrolysis towards an economically viable technology to produce synthetic fuels and chemical precursors.

Acknowledgments

This work has received funding from the ETH Board in the framework of the Joint Strategic Initiative "Synthetic Fuels from Renewable Resources". This work was partially supported by the NCCR Catalysis (grant number 180544), a National Centre of Competence in Research funded by the Swiss National

Science Foundation. The NMR hardware was partially granted by the Swiss National Science Foundation (SNSF, grant no. 206021_150638/1). The authors acknowledge the support of the Scientific Center for Optical and Electron Microscopy (ScopeM) of the ETH Zurich, and of Dr. Peng Zeng of the ScopeM for the FIB-SEM results.

Supporting Information Available: includes experimental methods, additional structural and microstructural characterizations by porosimetry, x-ray diffraction and scanning electrode microscopy, as well as chemical analysis and non-normalized faradaic efficiency data.

References

(1) Delbeke, J.; Runge-Metzger, A.; Slingenberg, Y.; Werksman, J. *The Paris Agreement*; Routledge, 2019. https://doi.org/10.4324/9789276082569-2.

(2) United Nations. 26th UN Climate Change Conference of the Parties 2021 - Glasgow Climate Pact https://unfccc.int/sites/default/files/resource/cma2021_10_add1_adv.pdf.

(3) Jermann, B.; Augustynski, J. Long-Term Activation of the Copper Cathode in the Course of CO_2 Reduction. *Electrochim. Acta* **1994**, *39* (11–12), 1891–1896. https://doi.org/10.1016/0013-4686(94)85181-6.

(4) Li, Y. C.; Zhou, D.; Yan, Z.; Gonçalves, R. H.; Salvatore, D. A.; Berlinguette, C. P.; Mallouk, T. E. Electrolysis of CO_2 to Syngas in Bipolar Membrane-Based Electrochemical Cells. *ACS Energy Lett.* **2016**, *1* (6), 1149–1153. https://doi.org/10.1021/acsenergylett.6b00475.

(5) Chen, Y.; Li, C. W.; Kanan, M. W. Aqueous CO_2 Reduction at Very Low Overpotential on Oxide-Derived Au Nanoparticles. *J. Am. Chem. Soc.* **2012**, *134* (49), 19969–19972. https://doi.org/10.1021/ja309317u.

(6) Senocrate, A.; Battaglia, C. Electrochemical CO_2 Reduction at Room Temperature: Status and Perspectives. *J. Energy Storage* **2021**, *36*, 102373. https://doi.org/10.1016/j.est.2021.102373.

(7) Hori, Y. Electrochemical CO_2 Reduction on Metal Electrodes. In *Modern Aspects of Electrochemistry*; Vayenas, C. G., White, R. E., Gamboa-Aldeco, M. E., Eds.; Springer: New York, NY, 2008; pp 89–189. https://doi.org/10.1007/978-0-387-49489-0_3.

(8) Hori, Y.; Kikuchi, K.; Suzuki, S. Production of CO and CH_4 in Electrochemical Reduction of CO_2 at Metal Electrodes in Aqueous Hydrogencarbonate Solution. *Chem. Lett.* **1985**, *14* (11), 1695–1698. https://doi.org/10.1246/cl.1985.1695.

(9) Verma, S.; Lu, X.; Ma, S.; Masel, R. I.; Kenis, P. J. A. The Effect of Electrolyte Composition on the Electroreduction of CO_2 to CO on Ag Based Gas Diffusion Electrodes. *Phys. Chem. Chem. Phys.* **2016**, *18* (10), 7075–7084. https://doi.org/10.1039/c5cp05665a.

(10) Marcandalli, G.; Goyal, A.; Koper, M. T. M. Electrolyte Effects on the Faradaic Efficiency of CO_2 Reduction to CO on a Gold Electrode. *ACS Catal.* **2021**, *11* (9), 4936–4945. https://doi.org/10.1021/acscatal.1c00272.

(11) Murata, A.; Hori, Y. Product Selectivity Affected by Cationic Species in Electrochemical Reduction of CO_2 and CO at a Cu Electrode. *Bull. Chem. Soc. Jpn.* **1991**, *64* (1), 123–127. https://doi.org/10.1246/bcsj.64.123.

(12) Monteiro, M. C. O.; Dattila, F.; Hagedoorn, B.; García-Muelas, R.; López, N.; Koper, M. T. M. Absence of CO_2 Electroreduction on Copper, Gold and Silver Electrodes without Metal Cations in Solution. *Nat. Catal.* **2021**, *4* (8), 654–662. https://doi.org/10.1038/s41929-021-00655-5.

(13) Zhang, Z.; Melo, L.; Jansonius, R. P.; Habibzadeh, F.; Grant, E. R.; Berlinguette, C. P. PH Matters When Reducing CO_2 in an Electrochemical Flow Cell. *ACS Energy Lett.* **2020**, *5* (10), 3101–3107. https://doi.org/10.1021/acsenergylett.0c01606.

(14) Chang, X.; Zhao, Y.; Xu, B. PH Dependence of Cu Surface Speciation in the Electrochemical CO Reduction Reaction. *ACS Catal.* **2020**, *10* (23), 13737–13747. https://doi.org/10.1021/acscatal.0c03108.

(15) Vennekoetter, J.-B.; Sengpiel, R.; Wessling, M. Beyond the Catalyst: How Electrode and Reactor Design Determine the Product Spectrum during Electrochemical CO_2 Reduction. *Chem. Eng. J.* **2019**, *364*, 89–101. https://doi.org/10.1016/j.cej.2019.01.045.

(16) Durst, J.; Rudnev, A.; Dutta, A.; Fu, Y.; Herranz, J.; Kaliginedi, V.; Kuzume, A.; Permyakova, A. A.; Paratcha, Y.; Broekmann, P.; Schmidt, T. J. Electrochemical CO_2 Reduction – A Critical View on Fundamentals, Materials and Applications. *Chim. Int. J. Chem.* **2015**, *69* (12), 769–776. https://doi.org/10.2533/chimia.2015.769.

(17) Burdyny, T.; Smith, W. A. CO_2 Reduction on Gas-Diffusion Electrodes and Why Catalytic Performance Must Be Assessed at Commercially-Relevant Conditions. *Energy Environ. Sci.* **2019**, *12* (5), 1442–1453. https://doi.org/10.1039/C8EE03134G.

(18) Verma, S.; Kim, B.; Jhong, H.-R. "Molly"; Ma, S.; Kenis, P. J. A. A Gross-Margin Model for Defining Technoeconomic Benchmarks in the Electroreduction of CO_2. *ChemSusChem* **2016**, *9* (15), 1972–1979. https://doi.org/10.1002/cssc.201600394.

(19) Verma, S.; Hamasaki, Y.; Kim, C.; Huang, W.; Lu, S.; Jhong, H. R. M.; Gewirth, A. A.; Fujigaya, T.; Nakashima, N.; Kenis, P. J. A. Insights into the Low Overpotential Electroreduction of CO_2 to CO on a Supported Gold Catalyst in an Alkaline Flow Electrolyzer. *ACS Energy Lett.* **2018**, *3* (1), 193–198. https://doi.org/10.1021/acsenergylett.7b01096.

(20) Dinh, C. T.; García De Arquer, F. P.; Sinton, D.; Sargent, E. H. High Rate, Selective, and Stable Electroreduction of CO_2 to Co in Basic and Neutral Media. *ACS Energy Lett.* **2018**, *3* (11), 2835–2840. https://doi.org/10.1021/acsenergylett.8b01734.

(21) García de Arquer, F. P.; Dinh, C.-T.; Ozden, A.; Wicks, J.; McCallum, C.; Kirmani, A. R.; Nam, D.-H.; Gabardo, C.; Seifitokaldani, A.; Wang, X.; Li, Y. C.; Li, F.; Edwards, J.; Richter, L. J.; Thorpe, S. J.; Sinton, D.; Sargent, E. H. CO_2 Electrolysis to Multicarbon Products at Activities Greater than 1 A Cm−2. *Science (80-.).* **2020**, *367* (6478), 661–666. https://doi.org/10.1126/science.aay4217.

(22) Larrazábal, G. O.; Strøm-Hansen, P.; Heli, J. P.; Zeiter, K.; Therkildsen, K. T.; Chorkendorff, I.; Seger, B. Analysis of Mass Flows and Membrane Cross-over in CO_2 Reduction at High Current Densities in an MEA-Type Electrolyzer. *ACS Appl. Mater. Interfaces* **2019**, *11* (44), 41281–41288. https://doi.org/10.1021/acsami.9b13081.

(23) Chen, Y.; Vise, A.; Klein, W. E.; Cetinbas, F. C.; Myers, D. J.; Smith, W. A.; Deutsch, T. G.; Neyerlin, K. C. A Robust, Scalable Platform for the Electrochemical Conversion of CO_2 to Formate: Identifying Pathways to Higher Energy Efficiencies. *ACS Energy Lett.* **2020**, *5* (6), 1825–1833. https://doi.org/10.1021/acsenergylett.0c00860.

(24) Corral, D.; Feaster, J. T.; Sobhani, S.; Deotte, J. R.; Lee, D. U.; Wong, A. A.; Hamilton, J.; Beck, V. A.; Sarkar, A.; Hahn, C.; Jaramillo, T. F.; Baker, S. E.; Duoss, E. B. Advanced Manufacturing for Electrosynthesis of Fuels and Chemicals from CO_2. *Energy Environ. Sci.* **2021**, *14* (5), 3064–3074. https://doi.org/10.1039/d0ee03679j.

(25) Dinh, C. T.; Burdyny, T.; Kibria, G.; Seifitokaldani, A.; Gabardo, C. M.; Pelayo García De Arquer, F.; Kiani, A.; Edwards, J. P.; De Luna, P.; Bushuyev, O. S.; Zou, C.; Quintero-Bermudez, R.; Pang, Y.; Sinton, D.; Sargent, E. H. CO_2 Electroreduction to Ethylene via Hydroxide-Mediated Copper Catalysis at an Abrupt Interface. *Science (80-.).* **2018**, *360* (6390), 783–787. https://doi.org/10.1126/science.aas9100.

(26) Ju, W.; Jiang, F.; Ma, H.; Pan, Z.; Zhao, Y.; Pagani, F.; Rentsch, D.; Wang, J.; Battaglia, C. Electrocatalytic Reduction of Gaseous CO_2 to CO on Sn/Cu-Nanofiber-Based Gas Diffusion Electrodes. *Adv. Energy Mater.* **2019**, *9* (32), 1901514. https://doi.org/10.1002/aenm.201901514.

(27) Leonard, M. E.; Clarke, L. E.; Forner-Cuenca, A.; Brown, S. M.; Brushett, F. R. Investigating Electrode Flooding in a Flowing Electrolyte, Gas-Fed Carbon Dioxide Electrolyzer. *ChemSusChem* **2020**, *13* (2), 400–411. https://doi.org/10.1002/cssc.201902547.

(28) Yang, K.; Kas, R.; Smith, W. A.; Burdyny, T. Role of the Carbon-Based Gas Diffusion Layer on Flooding in a Gas Diffusion Electrode Cell for Electrochemical CO_2 Reduction. *ACS Energy Lett.* **2021**, *6* (1), 33–40. https://doi.org/10.1021/acsenergylett.0c02184.

(29) De Jesus Gálvez-Vázquez, M.; Moreno-García, P.; Xu, H.; Hou, Y.; Hu, H.; Montiel, I. Z.; Rudnev, A. V.; Alinejad, S.; Grozovski, V.; Wiley, B. J.; Arenz, M.; Broekmann, P.; Moreno-García, P. Environment Matters: CO_2RR Electrocatalyst Performance Testing in a Gas-Fed Zero-Gap Electrolyzer. *ACS Catal.* **2020**, *10* (21), 13096–13108. https://doi.org/10.1021/acscatal.0c03609.

(30) Lu, Q.; Rosen, J.; Zhou, Y.; Hutchings, G. S.; Kimmel, Y. C.; Chen, J. G.; Jiao, F. A Selective and Efficient Electrocatalyst for Carbon Dioxide Reduction. *Nat. Commun.* **2014**, *5*, 1–6. https://doi.org/10.1038/ncomms4242.

(31) Dufek, E. J.; Lister, T. E.; McIlwain, M. E. Bench-Scale Electrochemical System for Generation of CO and Syn-Gas. *J. Appl. Electrochem.* **2011**, *41* (6), 623–631. https://doi.org/10.1007/s10800-011-0271-6.

(32) Gabardo, C. M.; Seifitokaldani, A.; Edwards, J. P.; Dinh, C. T.; Burdyny, T.; Kibria, M. G.; O'Brien, C. P.; Sargent, E. H.; Sinton, D. Combined High Alkalinity and Pressurization Enable Efficient CO_2 Electroreduction to CO. *Energy Environ. Sci.* **2018**, *11* (9), 2531–2539. https://doi.org/10.1039/c8ee01684d.

(33) Kong, Y.; Liu, M.; Hu, H.; Hou, Y.; Vesztergom, S.; Gálvez-Vázquez, M. de J.; Zelocualtecatl Montiel, I.; Kolivoška, V.; Broekmann, P. Cracks as Efficient Tools to Mitigate Flooding in Gas Diffusion Electrodes Used for the Electrochemical Reduction of Carbon Dioxide. *Small Methods* **2022**, *6* (9), 2200369. https://doi.org/10.1002/smtd.202200369.

(34) Wu, Y.; Garg, S.; Li, M.; Idros, M. N.; Li, Z.; Lin, R.; Chen, J.; Wang, G.; Rufford, T. E. Effects of Microporous Layer on Electrolyte Flooding in Gas Diffusion Electrodes and Selectivity of CO_2 Electrolysis to CO. *J. Power Sources* **2022**, *522*, 230998. https://doi.org/10.1016/j.jpowsour.2022.230998.

(35) Lee, S.; Park, J. S.; Lee, T. R. The Wettability of Fluoropolymer Surfaces: Influence of Surface Dipoles. *Langmuir* **2008**, *24* (9), 4817–4826. https://doi.org/10.1021/la700902h.

(36) Zhang, Y.; Yang, B.; Li, K.; Hou, D.; Zhao, C.; Wang, J. Electrospun Porous Poly(Tetrafluoroethylene-: Co -Hexafluoropropylene- Co -Vinylidene Fluoride) Membranes for Membrane Distillation. *RSC Adv.* **2017**, *7* (89), 56183–56193. https://doi.org/10.1039/c7ra09932k.

(37) Lee, J. H.; Kattel, S.; Xie, Z.; Tackett, B. M.; Wang, J.; Liu, C.-J.; Chen, J. G. Understanding the Role of Functional Groups in Polymeric Binder for Electrochemical Carbon Dioxide Reduction on Gold Nanoparticles. *Adv. Funct. Mater.* **2018**, *28* (45), 1804762. https://doi.org/10.1002/adfm.201804762.

(38) Liang, H. Q.; Zhao, S.; Hu, X. M.; Ceccato, M.; Skrydstrup, T.; Daasbjerg, K. Hydrophobic Copper Interfaces Boost Electroreduction of Carbon Dioxide to Ethylene in Water. *ACS Catal.* **2021**, *11* (2), 958–966. https://doi.org/10.1021/acscatal.0c03766.

(39) Dutta, A.; Morstein, C. E.; Rahaman, M.; Cedeno López, A.; Broekmann, P. Beyond Copper in CO_2 Electrolysis: Effective Hydrocarbon Production on Silver-Nanofoam Catalysts. *ACS Catal.* **2018**, *8* (9), 8357–8368. https://doi.org/10.1021/acscatal.8b01738.

(40) Veenstra, F. L. P.; Ackerl, N.; Martín, A. J.; Pérez-Ramírez, J. Laser-Microstructured Copper Reveals Selectivity Patterns in the Electrocatalytic Reduction of CO_2. *Chem* **2020**, *6* (7), 1707–1722. https://doi.org/10.1016/j.chempr.2020.04.001.

(41) Möller, T.; Ngo Thanh, T.; Wang, X.; Ju, W.; Jovanov, Z.; Strasser, P. The Product Selectivity Zones in Gas Diffusion Electrodes during the Electrocatalytic Reduction of CO_2. *Energy Environ. Sci.* **2021**, *14* (11), 5995–6006. https://doi.org/10.1039/D1EE01696B.

(42) Yang, K. D.; Ko, W. R.; Lee, J. H.; Kim, S. J.; Lee, H.; Lee, M. H.; Nam, K. T. Morphology-Directed Selective Production of Ethylene or Ethane from CO_2 on a Cu Mesopore Electrode. *Angew. Chemie - Int. Ed.* **2017**, *56* (3), 796–800. https://doi.org/10.1002/anie.201610432.

(43) Qiao, Y.; Lai, W.; Huang, K.; Yu, T.; Wang, Q.; Gao, L.; Yang, Z.; Ma, Z.; Sun, T.; Liu, M.; Lian, C.; Huang, H. Engineering the Local Microenvironment over Bi Nanosheets for Highly Selective Electrocatalytic Conversion of CO_2 to HCOOH in Strong Acid. *ACS Catal.* **2022**, *12* (4), 2357–2364. https://doi.org/10.1021/acscatal.1c05135.

(44) Monteiro, M. C. O.; Dieckhöfer, S.; Bobrowski, T.; Quast, T.; Pavesi, D.; Koper, M. T. M.; Schuhmann, W. Probing the Local Activity of CO_2 Reduction on Gold Gas Diffusion Electrodes: Effect of the Catalyst Loading and CO_2 Pressure. *Chem. Sci.* **2021**, *12* (47), 15682–15690. https://doi.org/10.1039/D1SC05519D.

(45) Joshi, P. B.; Karki, N.; Wilson, A. J. Electrocatalytic CO_2 Reduction in Acetonitrile Enhanced by the Local Environment and Mass Transport of H_2O. *ACS Energy Lett.* **2022**, *7* (2), 602–609. https://doi.org/10.1021/acsenergylett.1c02667.

(46) Suter, S.; Haussener, S. Optimizing Mesostructured Silver Catalysts for Selective Carbon Dioxide Conversion into Fuels. *Energy Environ. Sci.* **2019**, *12* (5), 1668–1678. https://doi.org/10.1039/c9ee00656g.

(47) Nesbitt, N. T.; Burdyny, T.; Simonson, H.; Salvatore, D.; Bohra, D.; Kas, R.; Smith, W. A. Liquid-Solid Boundaries Dominate Activity of CO_2 Reduction on Gas-Diffusion Electrodes. *ACS Catal.* **2020**, *10* (23), 14093–14106. https://doi.org/10.1021/acscatal.0c03319.

(48) Xing, Z.; Hu, L.; Ripatti, D. S.; Hu, X.; Feng, X. Enhancing Carbon Dioxide Gas-Diffusion Electrolysis by Creating a Hydrophobic Catalyst Microenvironment. *Nat. Commun.* **2021**, *12* (1), 1–11. https://doi.org/10.1038/s41467-020-20397-5.

(49) Hori, Y.; Takahashi, R.; Yoshinami, Y.; Murata, A. Electrochemical Reduction of CO at a Copper Electrode. *J. Phys. Chem. B* **1997**, *101* (36), 7075–7081. https://doi.org/10.1021/jp970284i.